Dyes and Pigments 170 (2019) 107578

Contents lists available at ScienceDirect

Dyes and Pigments

journal homepage: www.elsevier.com/locate/dyepig

Aminostyrylquinoxalines derived organic materials with remarkable solvatochromic and mechanofluorochromic properties

Jia Yu[a,1], Zhifang Liu[a,1], Bowei Wang[a,b,c,**], Yuqi Cao[a], Dongqi Liu[a], Fuchao Li[a], Xilong Yan[a,b,c,*]

[a] School of Chemical Engineering and Technology, Tianjin University, Tianjin, 300350, PR China
[b] Collaborative Innovation Center of Chemical Science and Engineering (Tianjin), Tianjin, 300072, PR China
[c] Tianjin Engineering Research Center of Functional Fine Chemicals, Tianjin, PR China

A R T I C L E I N F O

Keywords:
2,3-Dimethylquinoxaline
Solvatochromism
Intramolecular charge transfer
Aggregation-induced emission
High contrast mechanofluorochromism

A B S T R A C T

Four multi-responsive fluorophores (**DMQA$_1$**, **DMQA$_2$**, **DMQB$_1$**, **DMQB$_2$**) based on 2,3-dimethylquinoxaline were successfully designed and synthesized. It was found that all these fluorophores presented remarkable red-shifted solvatochromic behavior with increasing solvent polarity, in which, **DMQA$_2$** displayed 117 nm red-shift from cyclohexane to DCM. Interestingly, these four compounds all exhibited high contrast mechano-fluorochromism and **DMQA$_2$** received the largest MFC spectral shift ($\Delta\lambda_{MFC}$ = 84 nm). Moreover, Power wide-angle X-ray diffraction (PXRD) and Differential scanning calorimetry (DSC) were carried out to clarify the crystalline-amorphous transformation upon grinding. In this work, the quinoxaline template was introduced to develop high-performance MFC materials.

1. Introduction

Multi-responsive organic fluorescent materials have received tremendous attention for their potential applications as pressure sensors [1], security ink [2], and water detectors in organic solvents [3,4]. However, most conventional luminogens suffer from the infamous aggregation-caused quenching (ACQ) effect [5], which hinders their further applications to a great extent.

Luckily, Tang et al. reported the aggregation-induced emission (AIE) phenomenon of 1-methyl-1,2,3,4,5-pentaphenylsilole, which emits extremely weak fluorescence in pure solutions but several times enhanced emission in solid state [6]. Luminescent materials with AIE properties have fundamentally overcome the limitation of ACQ effect and arise extensive research interest [7–10]. In 2010, Park firstly designed the mechanofluorochromic (MFC) materials based on AIE property [11]. Combining the advantage of both AIE and MFC materials, series AIE-active MFC templates such as distyrylanthrancene derivatives [12], triphenylamine derivatives [13], silole derivatives [14], tetraphenylethene (TPE) derivatives [15], cyano-substituted diarylethene derivatives [11] and pyrone derivatives [16] have been explored. Nevertheless, few AIE-active MFC materials have been designed based on flattened quinoxaline derived templates and only a tiny part of them displayed high contrast MFC behavior. Moreover, the majority of these reported MFC materials experienced a tedious and complex synthesis routine, which takes up too much time of researchers [17]. Therefore, exploring simple and short synthesis routines for developing high contrast MFC materials is still of great challenge.

In this work, we introduced four luminophores (**DMQs**) based on 2,3-dimethylquinoxaline with phenothiazine or carbazole as electron donor in only three steps, respectively (Scheme 1). These targeted compounds exhibited significant mechanofluorochromic and solvatochromic properties. For instance, the maximum emission peaks of **DMQA$_1$**, **DMQA$_2$**, **DMQB$_1$**, and **DMQB$_2$** experienced 42 nm, 84 nm, 30 nm, and 37 nm red-shift, respectively, upon grinding. It should be noted that our work has enriched AIE-active MFC templates and provided new members to high- performance MFC materials.

2. Experimental

2.1. Materials and characterizations

All these raw materials and reagents were purchased from commercial sources. ^{1}H NMR (400 MHz) and ^{13}C NMR (100 MHz) spectra were measured on a Bruker Avance (III) spectrometer with $CDCl_3$ as the solvent. High resolution mass spectrum was acquired on Bruker Daltonics micrOTOF-Q II instrument. UV–vis spectra were recorded by

* Corresponding author. School of Chemical Engineering and Technology, Tianjin University, Tianjin, 300350, PR China.
** Corresponding author. School of Chemical Engineering and Technology, Tianjin University, Tianjin, 300350, PR China.
E-mail addresses: bwwang@tju.edu.cn (B. Wang), yan@tju.edu.cn (X. Yan).
[1] These authors contributed equally to this work.

https://doi.org/10.1016/j.dyepig.2019.107578
Received 18 March 2019; Received in revised form 21 May 2019; Accepted 21 May 2019
Available online 13 June 2019
0143-7208/

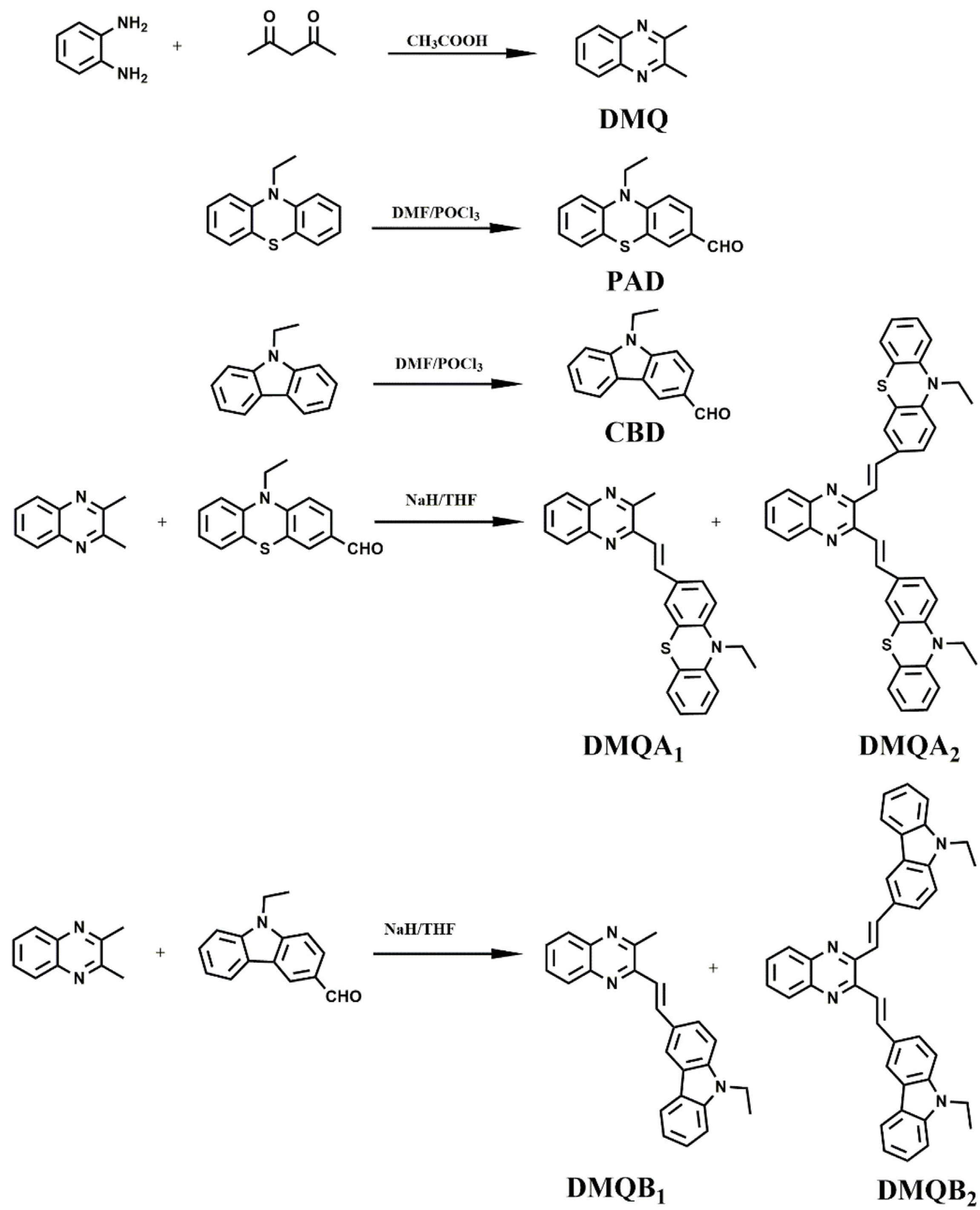

Scheme 1. Synthesis routes of **DMQA$_1$**, **DMQA$_2$**, **DMQB$_1$** and **DMQB$_2$**.

using Evolution 300 spectrophotometer. Photoluminescence spectra of liquid and Photoluminescence spectra of solid-state were performed on Hitachi F-2500 spectrophotometer and Horiba Jobin Yvon Fluorolog-3 spectrophotometer, respectively. Thermal gravimetric analysis (TGA) was measured on an STA 409 PC with a heating rate of 10 °C/min from room temperature to 800 °C in a stream of nitrogen (40 mL/min). Differential scanning calorimetry (DSC) was carried out on a Perkin-Elmerat and the heating rate is 10 °C/min under N_2 atmosphere. The XRD measurements were measured on a Bruker D8 Focus Powder X-ray diffraction instrument with the Cu K_α source radiation at room temperature. Data points were obtained at a scanning rate of 5°/min from $2\theta = 5°–60°$. Single crystal X-ray diffraction (SXRD) data were characterized on a Bruker AXS Smart APEX II diffractometer. The structure was solved with direct methods by the SHELXL-97 programs. Element analysis was carried on VarioEL cube and the IR spectra of these compounds were characterized on a Nicolet 380 FT-IR spectrometer.

2.2. Synthesis

10-methyl-10*H*-phenothiazine [18] and 9-ethyl-9*H*-carbazole [19] were synthesized as the literature reported.

*2.2.1. Synthesis of 2,3-dimethylquinoxaline (**DMQ**)*

2,4-Pentanedione (0.50 mmol) and 1, 2-phenylendiamine (0.55 mmol) were added into glacial CH_3COOH (4.0 mL). The solution was stirred at 60 °C for 2 h. Then, the mixture was poured into ice and extracted with 1,2-dichloromethane. The organic layer was dried with Na_2SO_4 and purified with silica-gel column chromatography using petroleum ether/ethyl acetate (v:v = 5:1) as eluent [20].

*2.2.2. Synthesis of 10-ethyl-10H-phenothiazine-3-carbaldehyede (**PAD**)*

As reported in the literature [21], 1.6 mL Phosphorus oxychloride was added into 5.0 mL N,*N*-Dimethylformamide dropwise at 0 °C under continuous stirring for 40 min. After the brown-red mixture was formed, 10-methyl-10*H*-phenothiazine (3.40 g, 16.00 mmol) in 20 mL DMF was added dropwise in ice-bath under vigorous stirring, and then the reaction mixture was heated at 60 °C for 14 h. After that, the red reaction-mixture was poured into ice slowly and the pH of the solution was adjusted to 7.0 using sodium hydroxide. The organic layer was extracted with dichloromethane and dried over anhydrous magnesium sulfate. Then, the solution was removed by vacuum evaporation and the residue was purified with silica-gel column chromatography using petroleum ether/ethyl acetate (v:v = 6:1) as eluent. Yellow powder was obtained. Yield: 85%.

*2.2.3. Synthesis of 10-ethyl-10H-carbazole-3-carbaldehyede (**CBD**)*

The synthesis process of 10-ethyl-10*H*-carbazole-3-carbaldehyede is similar to that of 10-ethyl-10*H*-phenothiazine-3-carbaldehyede. White powder was obtained. Yield: 83% [22].

*2.2.4. Synthesis of 10-ethyl-3-(2-(3-methylquinoxaline-2-yl)-10H-pehnothiazine (**DMQA$_1$**)*

THF (5 mL) was slowly added into the mixture of NaH (70%, 0.15 g, 4.50 mmol) and 2,3-dimethylquinoxaline (0.63 g, 4.00 mmol) at 0 °C under vigorous stirring for 45 min. After that, the 10-ethyl-10*H*-phenothiazine-3-carbaldehyede (1.00 g, 4.00 mmol) in THF solution was added dropwise. The mixture was stirred at room temperature under nitrogen atmosphere for 16 h and poured into ice, then neutralized with 5% HCl solution. After extracted with 1,2-dichloromethane and washed with water, the organic layer was separated with silica-gel column chromatography using petroleum ether/1,2-dichloromethane (v:v = 1:2) as eluent. Yellow product was obtained after recrystallization. Yield: 62%; m.p. 171–174 °C; ^{1}H NMR (400 MHz, $CDCl_3$) δ 8.09–8.00 (m, 1H), 7.99–7.87 (m, 2H), 7.75–7.58 (m, 2H), 7.43 (d, *J* = 16.5 Hz, 2H), 7.33 (s, 1H), 7.21–7.09 (m, 2H), 6.99–6.82 (m, 3H), 3.96 (d, *J* = 6.1 Hz, 2H), 2.87 (s, 3H), 1.45 (t, *J* = 7.0 Hz, 3H). ^{13}C NMR (100 MHz, $CDCl_3$) δ 152.55, 149.91, 145.64, 144.15, 141.53, 141.12, 136.29, 130.86, 129.10, 128.92, 128.81, 128.28, 127.67, 127.42, 125.63, 124.53, 123.54, 122.71, 120.55, 115.16, 114.92, 42.05, 23.16, 12.96. HRMS (ESI): calcd. for $C_{25}H_{21}N_3S$: 396.1529 $(M + H)^+$, found 396.1535. Elemental analysis calcd (%) for $C_{25}H_{21}N_3S$: C, 75.92; H, 5.35; N, 10.62; S, 8.11. Found: C, 75.33; H, 5.35; N, 10.36; S, 8.02.

*2.2.5. Synthesis of 2,3-bis-2-(10H-ethyl-10H-phenothiazin-3-yl-vinyl) quinoxaline (**DMQA$_2$**)*

The synthesis of **DMQA$_2$** is similar to that of **DMQA$_1$**, **DMQA$_2$** was obtained from 2,3-dimethylquinoxaline (0.63 g, 4.00 mmol) and 10-ethyl-10*H*-phenothiazine-3-carbaldehyede (2.00 g, 8.00 mmol) with NaH (70%, 0.31 g, 9.00 mmol) as the base. The crude product was purified with petroleum ether/1,2-dichloromethane (v:v = 1:2) as eluent. Light orange product was obtained. Yield: 43%; m.p. 216–218 °C; ^{1}H NMR (400 MHz, $CDCl_3$): δ 8.00 (dt, *J* = 16.5, 3.2 Hz, 2H), 7.88 (d, *J* = 15.5 Hz, 2H), 7.69–7.61 (m, 2H), 7.47 (dd, *J* = 11.6, 9.9 Hz, 6H), 7.20–7.12 (m, 4H), 6.94–6.87 (m, 6H), 3.97 (q, *J* = 7.0 Hz, 4H), 1.46 (t, *J* = 7.0 Hz, 6H); ^{13}C NMR (100 MHz, $CDCl_3$) δ 149.17, 145.55, 144.21, 141.56, 136.65, 130.99, 129.23, 128.78, 127.46, 127.44, 127.39, 125.91, 124.45, 123.61, 122.67, 120.58, 115.14, 114.96, 42.06, 12.99. HRMS (ESI): calcd. for $C_{40}H_{32}N_4S_2$: 633.2136 $(M + H)^+$, found 633.2135. Elemental analysis calcd (%) for $C_{40}H_{32}N_4S_2$: C, 75.92; H, 5.10; N, 8.85; S, 10.13. Found: C, 75.60; H, 4.941; N, 8.82; S, 10.451.

*2.2.6. Synthesis of 9-ethyl-3-(2-(3-methylquinoxaline-2-yl) vinyl-9H-carbazole (**DMQB$_1$**)*

By following the synthesis procedure of **DMQA$_1$**, **DMQB$_1$** was obtained. The crude product was purified with petroleum ether/1,2-dichloromethane (v:v = 1:3) as eluent. Yellow-green product was obtained. Yield: 68%; m.p. 122–125 °C; ^{1}H NMR (400 MHz, $CDCl_3$) δ 8.04 (dd, *J* = 16.2, 7.5 Hz, 3H), 7.84 (d, *J* = 7.8 Hz, 1H), 7.78–7.64 (m, 2H), 7.43 (t, *J* = 7.6 Hz, 1H), 7.36 (d, *J* = 8.1 Hz, 1H), 7.23–7.09 (m, 4H), 6.80 (d, *J* = 12.4 Hz, 1H), 4.28 (q, *J* = 7.1 Hz, 2H), 2.56 (s, 3H), 1.37 (t, *J* = 7.1 Hz, 3H). ^{13}C NMR (100 MHz, $CDCl_3$) δ 152.60, 150.40, 141.65, 141.04, 140.66, 140.46, 138.81, 129.04, 128.82, 128.69, 128.28, 127.68, 126.12, 125.53, 123.44, 122.98, 120.62, 120.38, 119.60, 119.41, 108.80, 37.76, 23.28, 13.90. HRMS (ESI): calcd. for $C_{25}H_{21}N_3$: 364.1803 $(M + H)^+$, found 364.1806. Elemental analysis calcd (%) for $C_{25}H_{21}N_3$: C, 82.61; H, 5.82; N, 11.56. Found: C, 80.34; H, 6.03; N, 11.44.

*2.2.7. Synthesis of 2,3-bis-2-(9H-ethyl-9H-carbazol-3-yl) vinyl) quinoxaline (**DMQB$_2$**)*

Similar to the synthesis procedure of **DMQA$_2$**, **DMQB$_2$** was synthesized. The crude product was purified with petroleum ether/1,2-dichloromethane (v:v = 1:2) as eluent. Green product was obtained. Yield: 35%; m.p. 300–301 °C; ^{1}H NMR (400 MHz, $CDCl_3$) δ 8.45 (s, 2H), 8.26 (d, *J* = 15.5 Hz,2H), 8.18 (d, *J* = 7.7 Hz, 2H), 8.13–8.04 (m, 2H), 7.89 (dd, *J* = 8.5, 1.4 Hz, 2H), 7.77 (d, *J* = 15.5 Hz, 2H), 7.72–7.63 (m, 2H), 7.55–7.40 (m, 6H), 7.33–7.20 (m, 2H), 4.41 (q, *J* = 7.2 Hz, 4H), 1.48 (t, *J* = 7.2 Hz, 6H). ^{13}C NMR (100 MHz, $CDCl_3$) δ 149.79, 141.58, 140.57, 140.46, 138.99, 129.01, 128.77, 127.93, 126.08, 125.53, 123.43, 123.02, 120.69, 120.43, 120.09, 119.37, 108.82, 108.78, 37.79, 13.84. HRMS (ESI): calcd. for $C_{40}H_{32}N_4$: 569.2694 $(M + H)^+$, found 569.2699. Elemental analysis calcd (%) for $C_{40}H_{32}N_4$: C, 84.48; H, 5.67; N, 9.85. Found: C, 80.92; H, 5.886; N, 9.46.

3. Results and discussion

3.1. Synthesis

DMQs were synthesized from the condensation between **DMQ**, phenothiazine and carbazole derivatives. NMR spectroscopy and high-resolution mass spectrometry were employed to confirm the structures of the four compounds (Figs. S1, S2, S3 and S4 ESI).

3.2. Photophysical property

As shown in Fig. S5, UV–vis absorption spectra of these four **DMQs** in DCM were quite similar. They all displayed two absorption peaks. The maximum absorption peak was attributed to the intramolecular charge transfer (ICT) transition and the other one was referred to the π-π* transition [23].

Considering their D-π-A structures and explicit ICT effect, solvatochromism performance was examined. As described in Fig. 1, these four fluorophores all exhibited fantastic solvatochromism. The emission of **DMQA$_1$**, **DMQA$_2$**, **DMQB$_1$**, and **DMQB$_2$** was located at 510 nm, 520 nm, 437 nm, 449 nm in cyclohexane and red-shifted to 599 nm, 637 nm, 522 nm, and 538 nm in DMF, respectively, accompanied with a quickly decreased emission intensity. Generally, this significant red-shift tendency can be explained by the larger polarity of the excited state than the ground state during π-π* transition process, which contributes to a greater solvent stabilization effect on the excited state [24].

As to gain further insight into the solvochromic properties of these compounds, their frontier orbital distributions were calculated with Gaussian 09. Depicted in Fig. 2, the highest occupied molecular orbitals

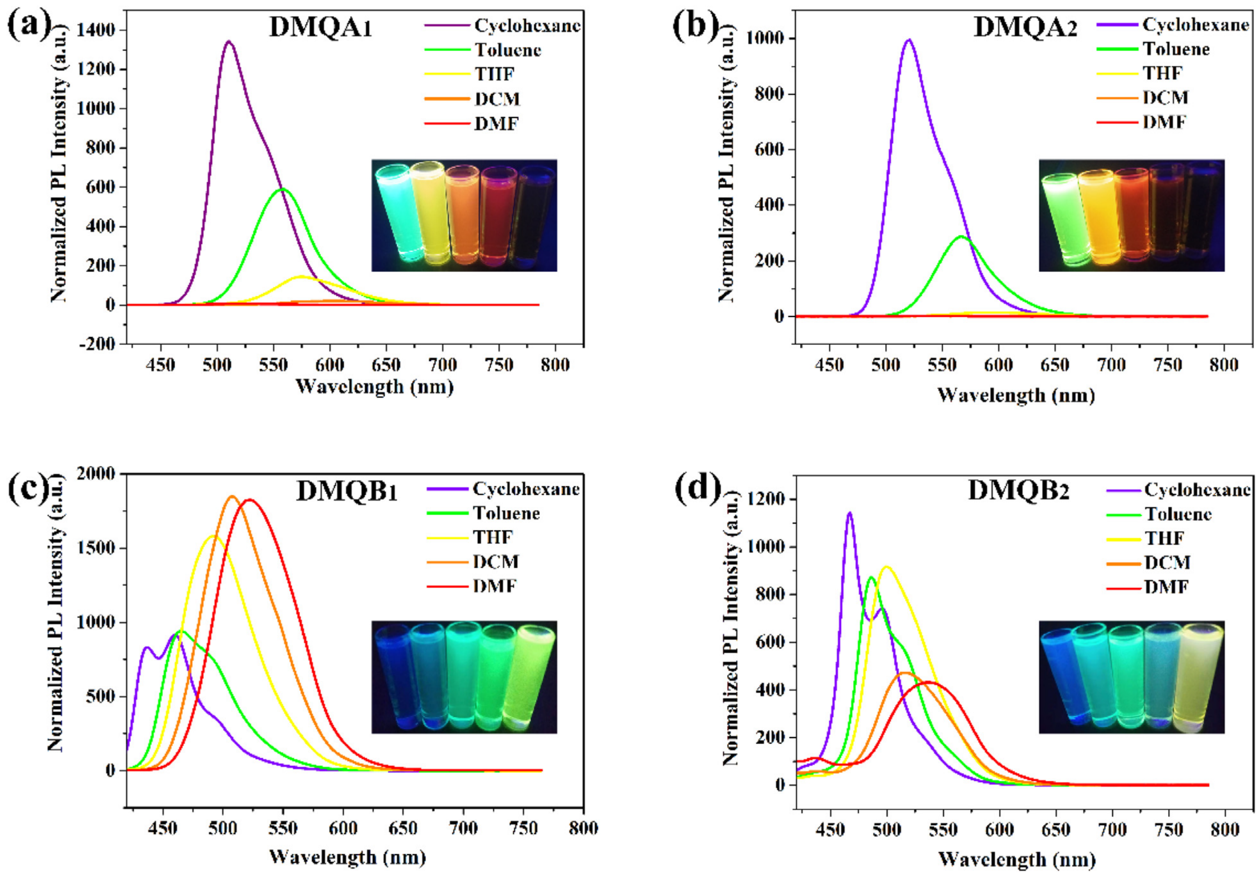

Fig. 1. The PL spectra in solvents with different polarity of (a) **DMQA$_1$** (b) **DMQA$_2$** (c) **DMQB$_1$** (d) **DMQB$_2$**. The concentration of the solutions is 1.0×10^{-4} mol L^{-1}.

(HOMOs) of **DMQA$_1$** and **DMQA$_2$** were mainly concentrated on phenothiazine unit while their lowest unoccupied molecular orbitals (LUMOs) were basically distributed on the 2,3-dimethylquinoxaline part. Such a distribution difference of HOMOs and LUMOs of **DMQA$_1$** and **DMQA$_2$** leads to a strong charge transfer and a narrow energy gap of 2.96 and 2.87 eV, respectively. However, the electron donor ability of carbazole is better than phenothiazine, which results in a different electrons distribution. The HOMOs of **DMQB$_1$** and **DMQB$_2$** were spread over the whole molecule while the LUMOs were mainly distributed on the 2,3-dimethyquinoxaline, leading to an energy gap of 3.38 and 3.17 eV, respectively. Such a large charge separation between D (donor) and A (acceptor) in these four molecules strongly sustained their

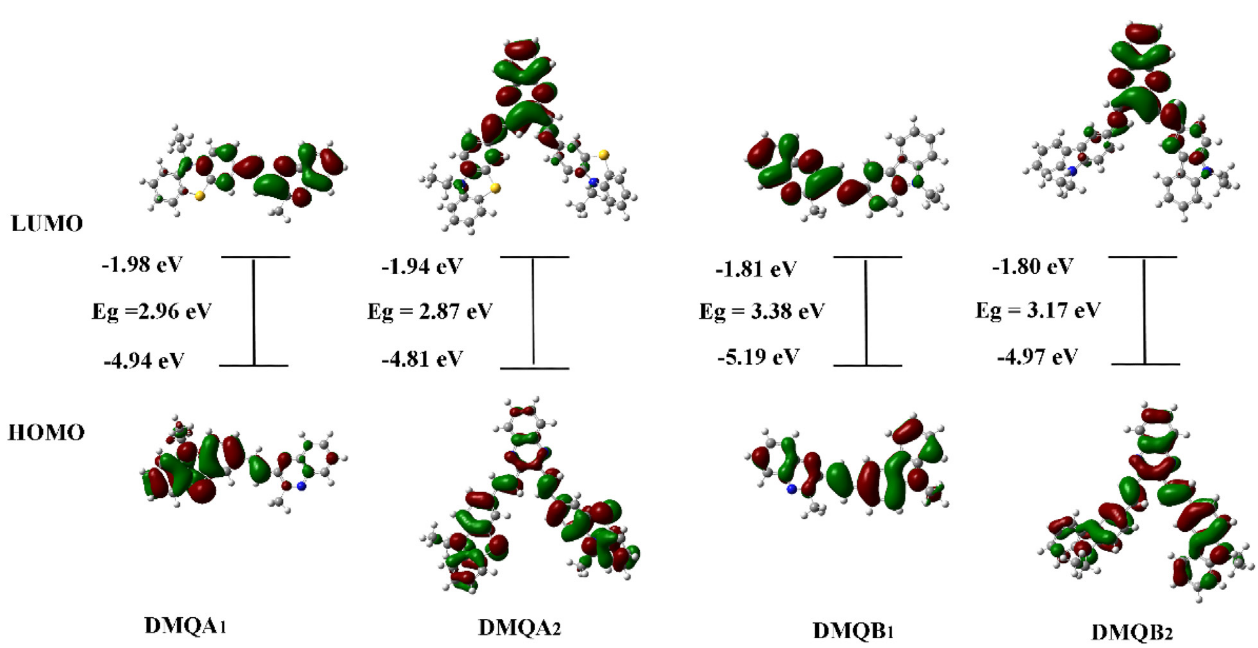

Fig. 2. B3LYP/6-31G(d) calculated molecular orbital amplitude plots and their calculated HOMO-LUMO energy gap (eV) of the four molecules.

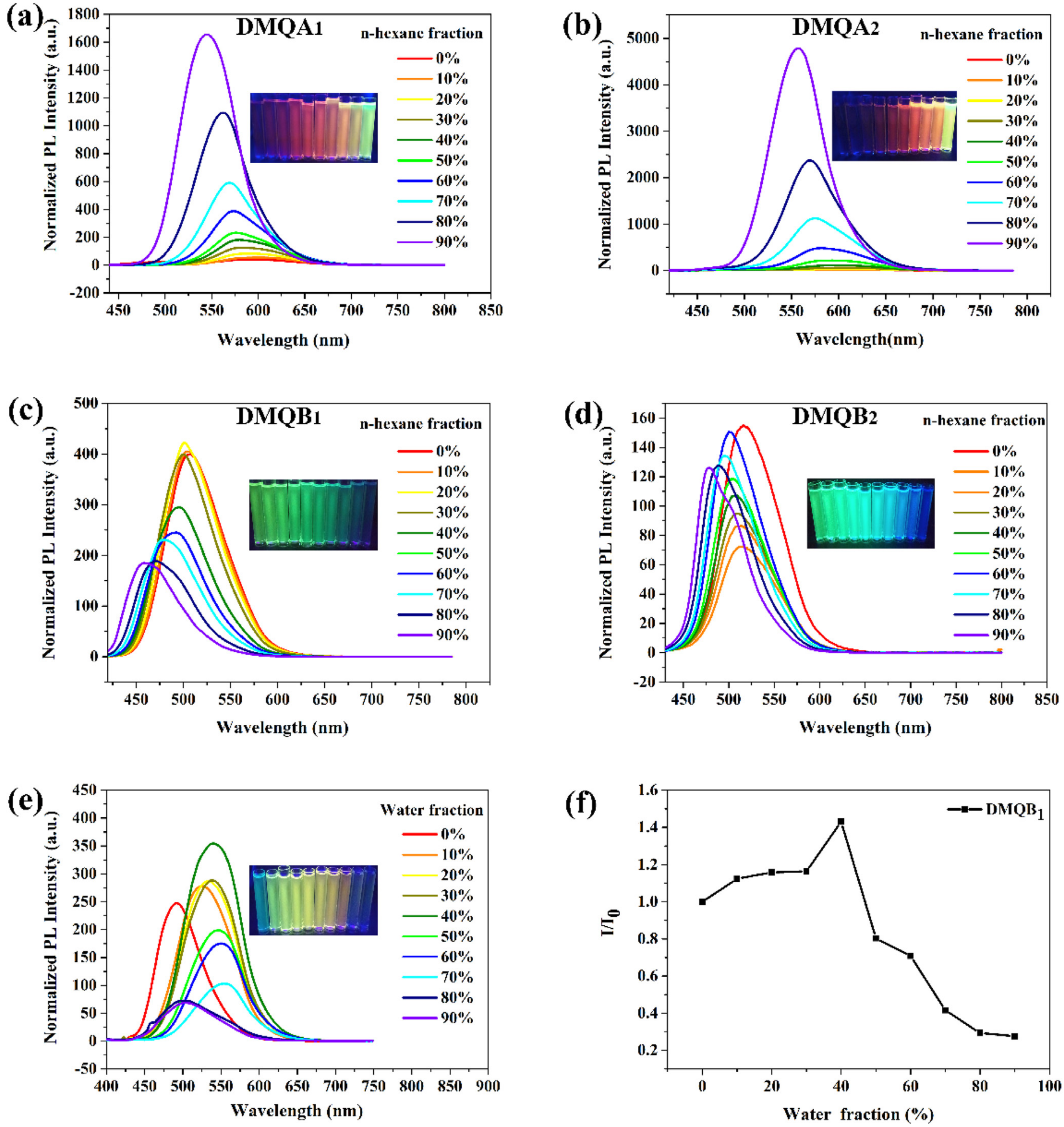

Fig. 3. Fluorescence spectra of the four compounds in DCM solution (a) **DMQA$_1$**; (b) **DMQA$_2$**; (c) **DMQB$_1$** and (d) **DMQB$_2$**. Insert pictures are photos of the solution with different *n*-hexane fraction under 365 nm UV lamp. (e) Fluorescence spectra of the **DMQB$_1$** in THF solution; (f) Plots of I/I$_0$ of the **DMQB$_1$**, I$_0$ refers to the PL intensity of 0% water fraction.

distinct ICT effect and narrower energy gap of **DMQA$_1$** and **DMQA$_2$** guaranteed their better solvochromism [25].

Fluorescence properties of these four compounds were characterized in DCM-*n*-hexane mixtures. As depicted in Fig. 3 and Fig. S7, the emission intensity of **DMQA$_1$**, **DMQA$_2$**, and **DMQB$_1$** increased upon addition of *n*-hexane, which can be ascribed to the restriction of intramolecular rotation (RIR) [26]. Different from **DMQA$_1$** and **DMQA$_2$**, the PL intensity of **DMQB$_1$** decreased when *n*-hexane fraction (f_n) exceeded 20%, which is probably attributed to the formation of amorphous particles [27]. The PL spectrum of **DMQB$_1$** was also characterized in THF-water mixture to get a further understand. As illustrated, the emission intensity firstly increased with the addition of water and reached the maximum value at 40% f_n and then decreased, corresponding to the phenomenon observed in DCM-*n*-hexane mixture. As for **DMQB$_2$**, the emission intensity declined when f_n was below 10% for the ICT effect and experienced an increase when f_n is between 10% and 60% for the RIR mechanism [23]. Along with the further addition of *n*-hexane, amorphous aggregation formed and the PL intensity declined again.

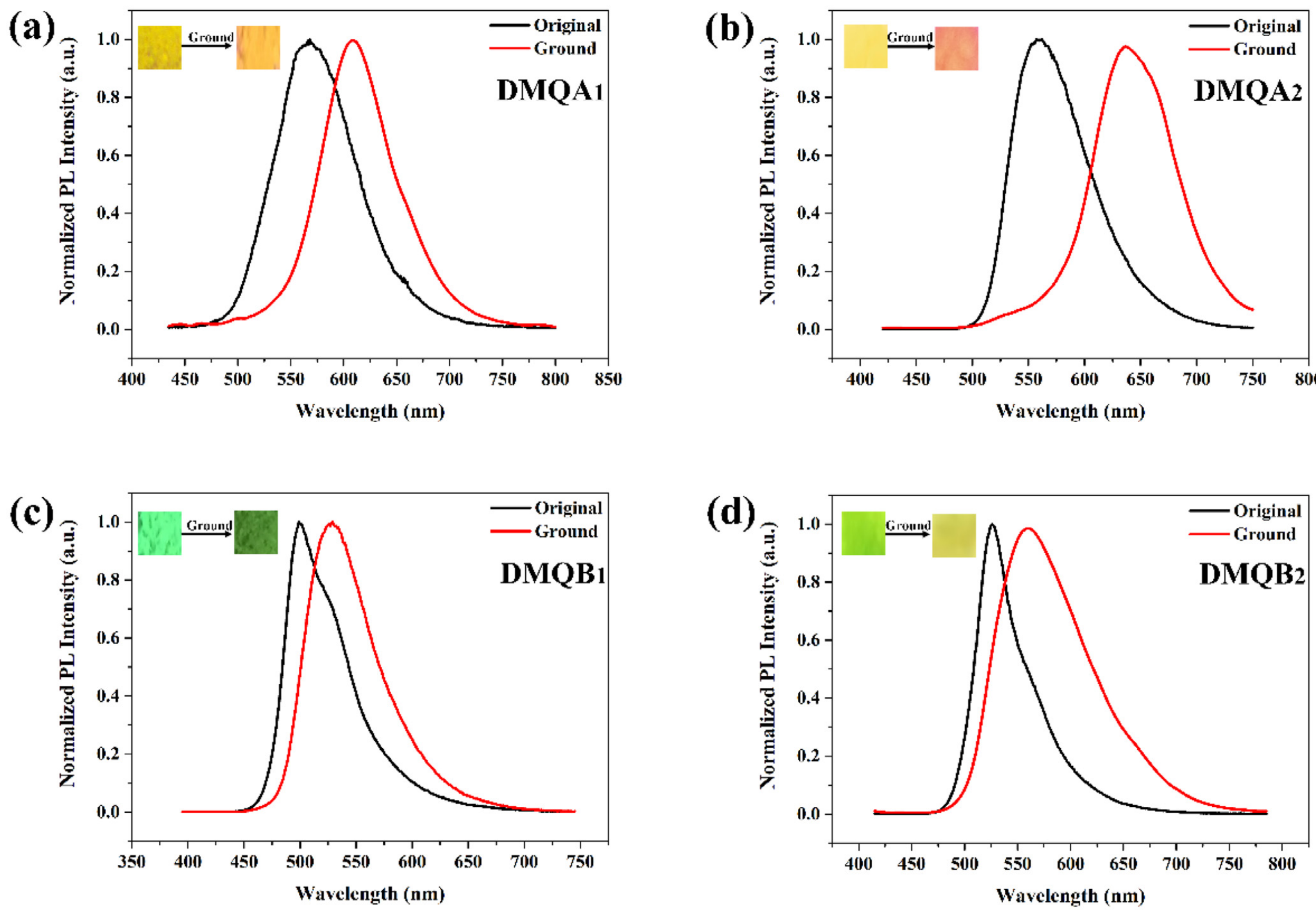

Fig. 4. PL spectra in solid states of the original and grounded samples. (a) **DMQA$_1$**; (b) **DMQA$_2$**; (c) **DMQB$_1$** and (d) **DMQB$_2$**.

3.3. Mechanofluorochromic properties

Then, the mechanofluorochromic properties of these **DMQs** were characterized. As described in Fig. 4 and Fig. 5, these four compounds all displayed distinct MFC properties. **DMQA$_1$**, **DMQA$_2$**, **DMQB$_1$** and **DMQB$_2$** emitted greenlish-yellow, yellow, blue-green, and green fluorescence in original state and changed to orange, red, dark green, light-yellow light upon grinding, accompanied with 42 nm, 84 nm, 30 nm, and 37 nm red-shift, respectively(Table S1, ESI). Generally, the red-shift of these four molecules can be attributed to the planarization induced by external force. These AIE molecules tend to adopt twisted configurations and loose packing modes in solid state and grinding will push the configuration planarization, thus leads to a bathochromic-shift in spectra. As for the better MFC properties of **DMQA$_1$** and **DMQA$_2$**, it can be explained by the more twisted bowl-shaped molecule configuration of phenothiazine [16,28].

To reveal the MFC mechanism, PXRD of these **DMQs** were characterized. As demonstrated in Fig. 6, both of original and ground samples presented sharp curves, except **DMQA$_2$**, implying their crystalline states. However, the intensity of the ground samples was weaker than the pristine, accompanied by several small peaks missing. This phenomenon can be explained by partial destruction of the crystalline state. As for **DMQA$_2$**, the curves of the original sample were sharp and strong while the peaks of the ground sample were almost flat, which was corresponded with the crystalline-amorphous transformation [12,17]. These results indicated that these compounds adopted two different packing mode before and after ground [29]. As has been reported [30], MFC properties were corresponded with the crystalline destruction and the transformation of molecule configuration. When external force was applied to the original sample, the crystal collapsed and transformed into a disordered amorphous state, which was further proved by the flattening and disappeared peaks in the XRD spectra [31].

According to Li et al. [10], the packing modes of these compounds have an inherent correlation with their MFC properties. However, it is hard to infer the packing mode in solid-state for the complicated affecting factors such as molecular configurations, special groups, electronic interactions [32]. Thus, single crystal is the most efficient and

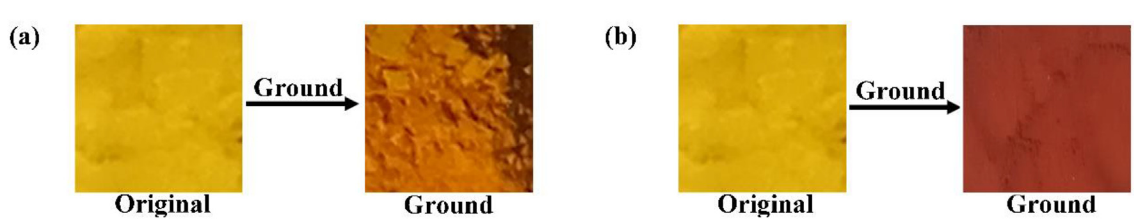

Fig. 5. Colors of the original and ground sample of (a) **DMQA$_1$** and (b) **DMQA$_2$** observed without the UV-lamp. (For interpretation of the references to colour in this figure legend, the reader is referred to the Web version of this article.)

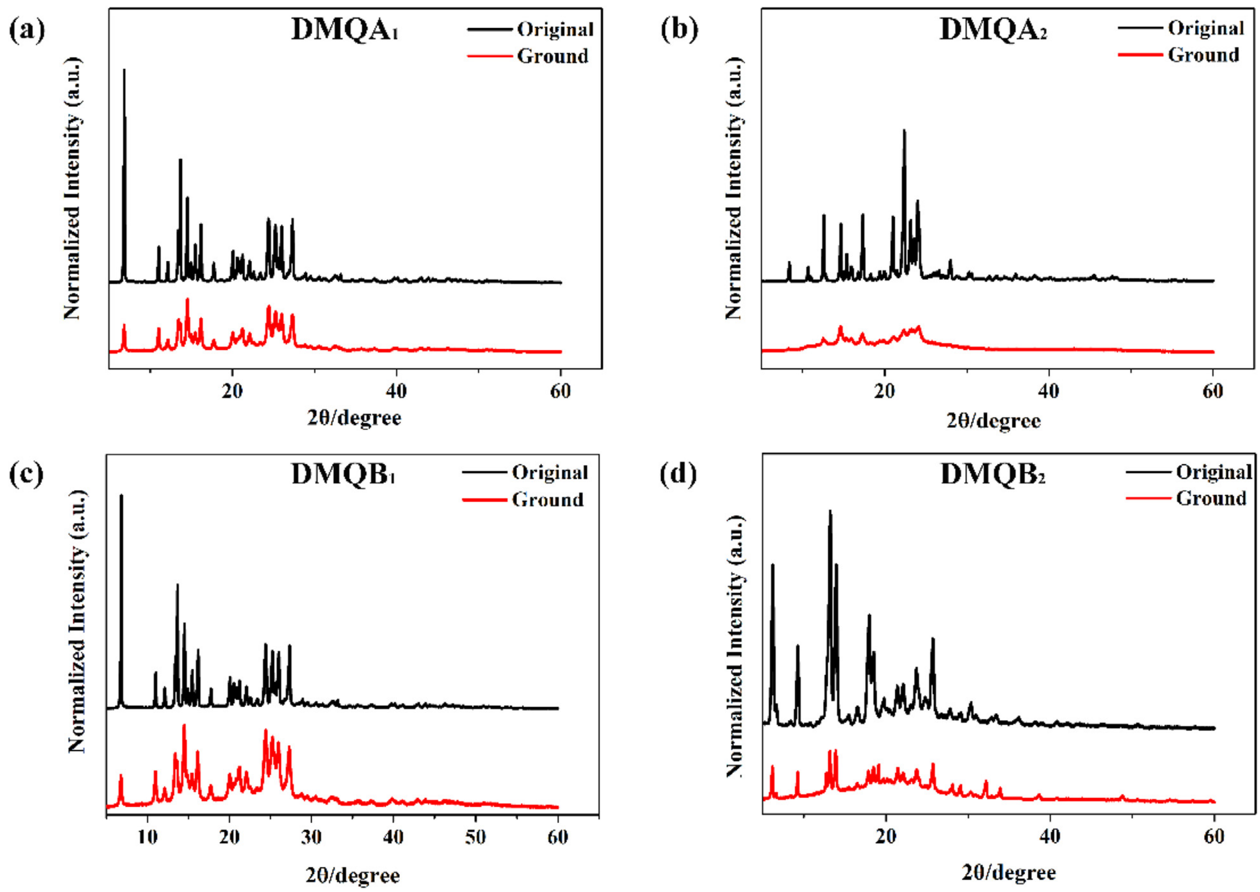

Fig. 6. XRD patterns of the original and grounded samples. (a) **$DMQA_1$**; (b) **$DMQA_2$**; (c) **$DMQB_1$** and (d) **$DMQB_2$**.

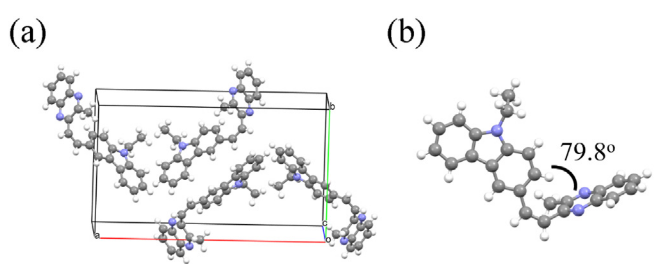

Fig. 7. (a) Single crystal and (b) basic unit of **$DMQB_1$**.

intensified way to clarify the packing mode and their MFC properties. We tried our best but only single crystal of **$DMQB_1$** was obtained in DCM/CH_3CN system and characterized. As shown in Fig. 7. and Table S2, the **$DMQB_1$** adopted a twisted conformation in crystal with torsion angles between the 2,3-dimethylquinoxaline template and the carbazole unit of 79.8°. The packing mode was very loose and it is hard to find face-to-face π-π staking between two molecules. Upon grinding, the dihedral angle decreased and molecular layers slipped, leading to planarization of the twisted configuration and increased π-π interaction. Thus, the discussed comprehensive factors contributed to the red-shifted MFC properties [33,34].

Furthermore, thermal properties of these **DMQs** were studied by DSC and TGA. Moreover, the DSC spectra of these four compounds were quite different. As illustrated in Fig. 8, both pristine and ground samples of **$DMQA_1$**, **$DMQA_2$**, and **$DMQB_2$** displayed two endothermic peaks in the spectra. The peak in the low-temperature zone referred to the crystalline to liquid crystal transition (T_L) and the peak in high-temperature zone was ascribed to the isotropic melt transition (T_m). In addition, the T_L of these samples was broader after grinding. Interestingly, the original sample of **$DMQB_2$** presented an extra exothermic peak at around 160 °C, which was referred to as the exothermic crystallization peak. As for **$DMQB_1$**, the original sample only exhibited a T_m peak while the ground sample presented an extra T_L before the T_m [12]. These results proved that the ground samples were in a more stable state and the pressing or grinding process brought morphology transformation, which was corresponded with the red-shifted MFC properties [31,35].

Based on the above discussion, we inferred that the better MFC properties of these phenothiazine substituted DMQs were attributed to their larger dihedral angle and the bowl shape configuration. As for the largest red-shift MFC property of $DMQA_2$ was also partly due to the completed packing mode transformation.

4. Conclusion

Four 2,3-dimethylquinoxaline derivatives, **$DMQA_1$**, **$DMQA_2$**, **$DMQB_1$** and **$DMQB_2$** were designed and synthesized. All these targeted **DMQs** displayed outstanding MFC properties, in which the phenothiazine substituted **DMQs** presented better MFC performance. This phenomenon is attributed to the more twisted bowl-shape configuration of phenothiazine unit. Moreover, these D-π-A type molecules also presented outstanding bathochromic solvatochromism for ICT effect and confirmed by DFT calculation. PXRD and DSC were carried out and indicated the intrinsic relationship between MFC properties and stacking patterns transformation upon grinding. Conclusively, our work enriched AIE-active MFC templates and introduced new members to high contrast MFC materials.

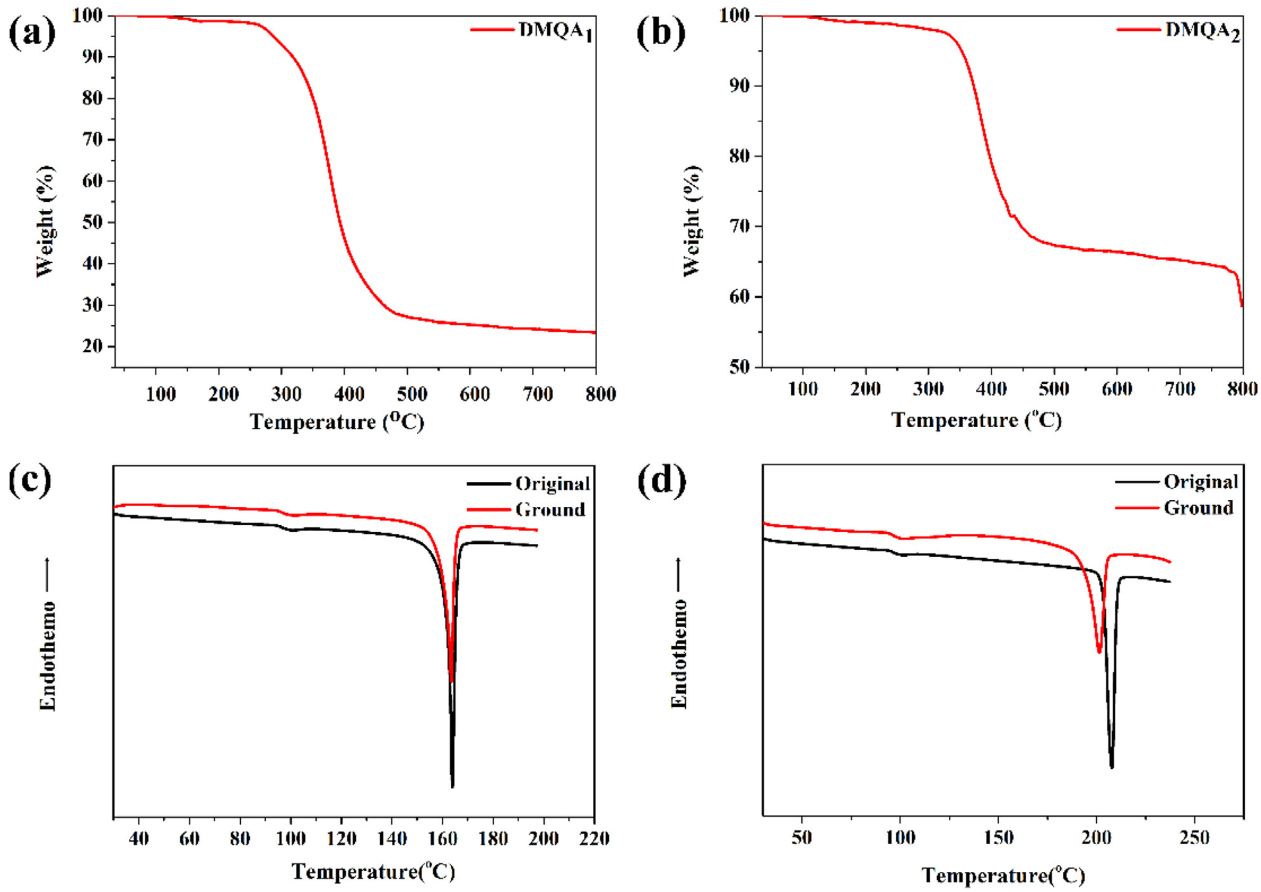

Fig. 8. TGA curves of (a) **DMQA$_1$** and (b) **DMQA$_2$**; DSC curves of (C) **DMQA$_1$** and (D) **DMQA$_2$**.

Conflicts of interest

The authors declare no conflict of interest.

Acknowledgements

This work was financially supported by the National Natural Science Foundation of China (Grant No. 21576194 and 21808161).

Appendix A. Supplementary data

Supplementary data to this article can be found online at https://doi.org/10.1016/j.dyepig.2019.107578.

References

[1] Shi P, Duan Y, Wei W, Xu Z, Li Z, Han T. A turn-on type mechanochromic fluorescent material based on defect-induced emission: implication for pressure sensing and mechanical printing. J Mater Chem C 2018;6(10):2476–82.
[2] Wu Z, Mo S, Tan L, Fang B, Su Z, Zhang Y, et al. Crystallization-induced emission enhancement of a deep-blue luminescence material with tunable mechano- and thermochromism. Small 2018;14(40):e1802524.
[3] Cao Y, Chen L, Liu D, Wang B. Multi-responsive red solid emitter: detection of trace water and sense of relative humidity. Sci China Mater 2019;62(6):823–30.
[4] Chen T, Chen Z, Gong W, Li C, Zhu M. Ultrasensitive water sensors based on fluorenone-tetraphenylethene AIE luminogens. Mater Chem Front 2017;1(9):1841–6.
[5] Shi J, Chang N, Li C, Mei J, Deng C, Luo X, et al. Locking the phenyl rings of tetraphenylethene step by step: understanding the mechanism of aggregation-induced emission. Chem Commun 2012;48(86):10675–7.
[6] Tang B, Zhan X, Yu G, Lee PPS, Liu Y, Zhu D. Efficient blue emission from siloles. J Mater Chem 2001;11(12):2974–8.
[7] Mei J, Huang Y, Tian H. Progress and trends in AIE-based bioprobes: a brief overview. ACS Appl Mater Interfaces 2018;10(15):12217–61.
[8] Ning Z, Chen Z, Zhang Q, Yan Y, Qian S, Cao Y, et al. Aggregation-induced emission (AIE)-active starburst triarylamine fluorophores as potential non-doped red emitters for organic light-emitting diodes and Cl_2 gas chemodosimeter. Adv Funct Mater 2007;17(18):3799–807.
[9] Gao Y, Feng G, Jiang T, Goh C, Ng L, Liu B, et al. Biocompatible nanoparticles based on diketo-PyrroloPyrrole (DPP) with aggregation-induced red/NIR emission for in vivo two-photon fluorescence imaging. Adv Funct Mater 2015;25(19):2857–66.
[10] Yang J, Ren Z, Chen B, Fang M, Zhao Z, Tang B, et al. Three polymorphs of one luminogen: how the molecular packing affects the RTP and AIE properties? J Mater Chem C 2017;5(36):9242–6.
[11] Yoon SJ, Chung JW, Gierschner J, Kim KS, Choi MG, Kim D, et al. Multistimuli two-color luminescence switching via different slip-stacking of highly fluorescent molecular sheets. J Am Chem Soc 2010;132(39):13675–83.
[12] Xiong Y, Yan X, Ma Y, Li Y, Yin G, Chen L. Regulating the piezofluorochromism of 9,10-bis(butoxystyryl)anthracenes by isomerization of butyl groups. Chem Commun 2015;51(16):3403–6.
[13] Cao Y, Xi W, Wang L, Wang H, Kong L, Zhou H, et al. Reversible piezofluorochromic nature and mechanism of aggregation-induced emission-active compounds based on simple modification. RSC Adv 2014;4(47):24649–52.
[14] Chang Z, Jing L, Wei C, Dong Y, Ye Y, Zhao Y, et al. Hexaphenylbenzene-based, pi-conjugated snowflake-shaped luminophores: tunable aggregation-induced emission effect and piezofluorochromism. Chem Eur J 2015;21(23):8504–10.
[15] Qiu Z, Zhao W, Cao M, Wang Y, Lam JWY, Zhang Z, et al. Dynamic visualization of stress/strain distribution and fatigue crack propagation by an organic mechanoresponsive AIE luminogen. Adv Mater 2018;30(44):e1803924.
[16] Cao Y, Xi Y, Teng X, Li Y, Yan X, Chen L. Alkoxy substituted D-π-A dimethyl-4-pyrone derivatives: aggregation induced emission enhancement, mechanochromic and solvatochromic properties. Dyes Pigments 2017;137:75–83.
[17] Yin G, Ma Y, Xiong Y, Cao X, Li Y, Chen L. Enhanced AIE and different stimuli-responses in red fluorescent (1,3-dimethyl)barbituric acid-functionalized anthracenes. J Mater Chem C 2016;4(4):751–7.
[18] Xue P, Yao B, Sun J, Xu Q, Chen P, Zhang Z, et al. Phenothiazine-based benzoxazole derivates exhibiting mechanochromic luminescence: the effect of a bromine atom. J Mater Chem C 2014;2(20):3942–50.
[19] Zhang Z, Tang L, Fan X, Wang Y, Zhang K, Sun Q, et al. N-Alkylcarbazoles: homolog manipulating long-lived room-temperature phosphorescence. J Mater Chem C 2018;6(33):8984–9.
[20] Tingoli M, Mazzella M, Panunzi B, Tuzi A. Chemlnform abstract: elemental iodine or diphenyl diselenide in the [Bis(trifluoroacetoxy)iodo]benzene-Mediated conversion of alkynes into 1,2-diketones. Eur J Org Chem 2011;2:399–404.
[21] Jia J, Wu Y. Alkyl length dependent reversible mechanofluorochromism of phenothiazine derivatives functionalized with formyl group. Dyes Pigments 2017;147:537–43.

[22] Meng F, Liu Y, Yu X, Lin W. A dual-site two-photon fluorescent probe for visualizing mitochondrial aminothiols in living cells and mouse liver tissues. New J Chem 2016;40(9):7399–406.
[23] Xi Y, Cao Y, Zhu Y, Guo H, Wu X, Li Y, et al. Mechanical stimuli induced emission spectra blue shift of two D-A type phenothiazine derivatives. Chem Lett 2018;47(5):650–3.
[24] Cao Y, Chen L, Xi Y, Li Y, Yan X. Stimuli-responsive 2,6-diarylethene-4*H*-pyran-4-one derivatives: aggregation induced emission enhancement, mechanochromism and solvatochromism. Mater Lett 2018;212:225–30.
[25] Guan X, Jia T, Zhang D, Zhang Y, Ma H, Lu D, et al. A new solvatochromic linear π-conjugated dye based on phenylene-(poly)ethynylene as supersensitive low-level water detector in organic solvents. Dyes Pigments 2017;136:873–80.
[26] Teng X, Wu X, Cao Y, Jin Y, Li Y, Yan X, et al. Piezochromic luminescence and aggregation induced emission of 9,10-bis[2-(2-alkoxynaphthalen-1-yl)vinyl]anthracene derivatives. Chin Chem Lett 2017;28(7):1485–91.
[27] Sun J, Yuan J, Li Y, Duan Y, Li Z, Du J, et al. Water-directed self-assembly of a red solid emitter with aggregation-enhanced emission: implication for humidity monitoring. Sensor Actuator B Chem 2018;263:208–17.
[28] Xu B, Mu Y, Mao Z, Xie Z, Wu H, Zhang Y, et al. Achieving remarkable mechanochromism and white-light emission with thermally activated delayed fluorescence through the molecular heredity principle. Chem Sci 2016;7(3):2201–6.
[29] Zhang X, Chi Z, Zhang J, Li H, Xu B, Li X, et al. Piezofluorochromic properties and mechanism of an aggregation-induced emission enhancement compound containing N-hexyl-phenothiazine and anthracene moieties. J Phys Chem B 2011;115(23):7606–11.
[30] Wang C, Xu B, Li M, Chi Z, Xie Y, Li Q, et al. A stable tetraphenylethene derivative: aggregation-induced emission, different crystalline polymorphs, and totally different mechanoluminescence properties. Mater Horiz 2016;3(3):220–5.
[31] Wang C, Li Z. Molecular conformation and packing: their critical roles in the emission performance of mechanochromic fluorescence materials. Mater Chem Front 2017;1(11):2174–94.
[32] Li Q, Li Z. The strong light-emission materials in the aggregated state: what happens from a single molecule to the collective group. Adv Sci 2017;4(7):1600484.
[33] Zhang G, Sun J, Xue P, Zhang Z, Gong P, Peng J, et al. Phenothiazine modified triphenylacrylonitrile derivates: AIE and mechanochromism tuned by molecular conformation. J Mater Chem C 2015;3(12):2925–32.
[34] Wu J, Cheng Y, Lan J, Wu D, Qan S, Yan L, et al. Molecular engineering of mechanochromic materials by programmed C-H arylation: making a counterpoint in the chromism trend. J Am Chem Soc 2016;138(39):12803–12.
[35] Okazaki M, Takeda Y, Data P, Pander P, Higginbotham H, Monkman A, et al. Thermally activated delayed fluorescent phenothiazine-dibenzo[a,j]phenazine-phenothiazine triads exhibiting tricolor-changing mechanochromic luminescence. Chem Sci 2017;8(4):2677–86.